2022 IEEE 33rd Annual International Symposium on Personal, Indoor and Mobile Radio Communications (PIMRC) | 978-1-6654-8053-6/22/$31.00 ©2022 IEEE | DOI: 10.1109/PIMRC54779.2022.9977460

Uplink Power Control and SNR-Dependent Beam Alignment Errors in MmWave Cellular Networks

Muhammad Saad Zia, Douglas M. Blough and Mary Ann Weitnauer
School of Electrical and Computer Engineering
Georgia Institute of Technology, Atlanta, Georgia 30332-0250, USA
Email: saad.zia@gatech.edu; doug.blough@ece.gatech.edu; mary.ann.weitnauer@ece.gatech.edu

***Abstract*—Beam alignment is a critical aspect in millimeter wave (mm-wave) cellular systems. However, the inherent limitations of channel estimation result in beam alignment errors, which degrade the system performance. For systems with a large number of antennas at the base station, downlink channel estimation is performed using uplink pilot signals. The beam alignment errors, thus, depend on the user equipment (UE) transmit power, which needs to be managed properly as the UEs are battery powered. This paper investigates how the use of uplink power control for the transmission of pilot signals in a mm-wave network affects the downlink beam alignment errors, which depend on various link parameters. We use stochastic geometry and statistics of the Student's *t*-distribution to develop an analytical model, which captures the interplay between the uplink power control and downlink signal-to-noise ratio (SNR) coverage probability. Our results indicate that using uplink power control significantly reduces UE power consumption without adversely affecting the downlink SNR coverage.**

***Index Terms*—Fractional power control, pilot signals, signal-to-noise ratio, beam alignment error, path-loss.**

I. Introduction

The millimeter-wave (mm-wave) frequencies are a promising solution to the spectrum crunch problem and can provide orders of magnitude increase in the data rates for the next generation of cellular systems [1]–[3]. However, the use of such frequencies brings about new practical challenges that are quite distinct from those of the traditionally used sub-6 GHz frequency bands. An important such challenge is the increased path-loss, caused by the sensitivity to blockages [4], [5].

The use of antenna arrays and an appropriate beamforming strategy is essential to counter the effects of high path-loss [6]. Antenna arrays make the transmissions directional by virtue of narrow beams whereas beamforming helps to direct the beams in the desired direction. Beamforming, however, requires channel state information (CSI), which can be obtained either through the use of a beam training process or by directly estimating the channel [7]. Both the approaches, however, have their limitations. Because of this impediment, beamforming suffers when the beam is not aligned exactly with the desired direction and, a suboptimal signal-to-noise ratio (SNR) on the desired link is realized. It is, therefore, extremely important to investigate the effects of such alignment errors on the system-level SNR of mm-wave cellular systems.

In cellular systems where the base stations (BSs) are equipped with a large number of antennas, the channel for downlink beamforming is estimated using uplink pilot signals transmitted by the user equipments (UEs) [8], [9]. This reduces the overhead associated with channel estimation. The UEs, however, are battery-constrained devices while, on the other hand, the accuracy of channel estimation depends on the SNR of the received pilot signals. A trade-off, thus, exists between the UE power consumption and the reliability of channel estimates. It is, therefore, of paramount importance to manage the power consumption of the UEs while ensuring that the SNR of uplink pilot signals is adequate enough to result in reliable channel estimates.

Power control mechanisms for the uplink transmissions have been proposed to manage the UE power consumption [10], [11]. The impact of power control on the system level performance of cellular systems has, however, been studied mostly for uplink data transmissions, e.g., [10]–[12] for sub-6 GHz systems and [13], [14] for mm-wave systems. On the other hand, power control for the transmission of uplink pilot signals has only been considered in some works, e.g., [8] for sub-6 GHz and [9] for mm-wave systems. Both of these works, however, focus on the issue of pilot contamination. To the best of the authors' knowledge, no prior work on mm-wave systems addresses how the downlink beam alignment errors, which arise from imperfect CSI, are affected when the power control is utilized for the transmission of uplink pilot signals.

This paper investigates the impact of uplink power control on the downlink SNR coverage probability of a mm-wave cellular network with imperfect beam alignment where the power control is utilized for the transmission of uplink pilot signals. The power savings on the UE side are also analyzed. Similar to our previous work [15], the beam alignment error is formulated as a function of the path-loss, blockage, and the antenna array characteristics. However, contrary to this paper, [15] considered a constant uplink transmit power. Our findings in this paper illustrate that the use of uplink power control can result in substantial power savings at the UE side without significantly compromising the downlink SNR coverage in the presence of beam alignment errors.

II. System Model

This paper considers a mm-wave cellular network in which the BS locations are modeled as an independent homogeneous Poisson point process (PPP) in the two-dimensional plane $\mathbb{R}^2$. The BS PPP is represented by Φ_{B} and its intensity by λ_{B}. The

downlink transmit power, P_{d}, of each BS is assumed to be constant.

To model the UE locations, an independent homogeneous PPP, Φ_u, with intensity λ_u is considered. To enable analytical tractability and the application of standard stochastic geometric techniques, it is assumed that a *typical UE* is stationed at the origin. The analysis is done for the typical UE as its presence does not disturb the overall statistics of the network [16]. The BS serving the typical UE is called the tagged BS.

An important aspect of mm-wave propagation is the susceptibility to blockages, which render the mm-wave links to be either in the line-of-sight (LOS) or the non-line-of-sight (NLOS) state. To emulate such blockage effects, this paper uses the generalized LOS ball blockage model of [2] because of its analytical simplicity, tractability and reliability in capturing the SINR statistics [5]. The ball model approximates the LOS region around a UE/BS by a ball of a certain fixed radius, R_B, which represents the maximum possible range for a LOS link. Within the radius R_B from the considered UE/BS, a link of length r can either be LOS with a probability $\mathcal{P}_{LOS}$, or NLOS with a probability $\mathcal{P}_{NLOS} = 1 - \mathcal{P}_{LOS}$. However, if the link distance is greater than R_B, then such a link is surely NLOS.

The path-loss for the LOS and the NLOS link states is modeled differently [1]. If the tagged BS is located at x, then the link length, r, for the typical UE can be written as $r = \|x\|$. Using the floating-intercept model, the path-loss for a link belonging to the k^{th} channel state, for $k \in \{LOS, NLOS\}$, is expressed as

$$L_k(r) = C_k r^{-\alpha_k}. \tag{1}$$

where α_k and C_k are the empirical path-loss parameters [3]. Further, it is assumed that the UE to BS associations are decided based on the maximum downlink received power criterion.

In this paper, antenna arrays are considered only at the BS side whereas a single isotropic antenna is assumed at each UE. Additionally, three sectors are considered at each BS to provide coverage, where each sector utilizes a uniform linear array (ULA) consisting of M directional antenna elements. Since the network is two-dimensional, beamforming is only considered along the azimuth plane while the elevation angle is kept constant at $\frac{\pi}{2}$. Each sector, thus, provides coverage in an angular region spanning $\left[-\frac{\pi}{3}, \frac{\pi}{3}\right]$ along the horizontal plane.

Moreover, we assume that each BS employs analog beamforming, where the antenna elements of the BS array are connected to a single radio frequency (RF) chain through phase-shifters [5]. Such a beamforming strategy has a low implementation complexity and cost; and results in a single communication beam. To serve a UE, the serving BS adjusts the weights of the phase-sifters correspondingly and spatially steers its beam towards the dominant propagation path for that specific UE [17]. To serve other UEs associated to it, the BS uses a scheduler. In this paper, round-robin scheduling of UEs is assumed.

The intrinsic properties of mm-wave propagation are captured well by a clustered channel model [4]. With analog beamforming, however, the dominant cluster is of paramount importance [18]. As a result, this paper only considers the dominant cluster between a UE and its serving BS, similar to [15]. The small-scale fading effects within the dominant cluster are modeled using the Nakagami distribution. For the LOS and the NLOS states, different Nakagami shape parameters are used [19]. Let N_{LOS} and N_{NLOS} represent the Nakagami shape parameters for the two channel states, respectively. Then, $N_{\text{LOS}} > N_{\text{NLOS}}$, and $N_k \in \mathbb{Z}^+$ for analytical tractability. Also, the fading on each link is assumed to be independent. The channel gain, ϱ_k, on each link due to the small-scale fading then becomes a normalized gamma random variable (RV).

For a BS to perform beamforming towards a specific UE, it requires the direction of the dominant propagation path between the BS and the UE is needed. In this paper, it is assumed that such information for downlink beamforming is estimated by the BS from the pilot signals that are transmitted by the UE [9]. However, channel estimation has its limitations, which result in beam alignment errors. The beam alignment error, ϵ, is modeled using a truncated Gaussian distribution with zero mean [20], [21]. Within a sector, the probability distribution function (PDF) of ϵ is expressed as [15]

$$f_\epsilon(y) = \frac{\sqrt{\frac{2}{\pi\sigma_\epsilon^2}}\exp\left(\frac{-y^2}{2\sigma_\epsilon^2}\right)}{\operatorname{erf}\left(\frac{\pi/3}{\sqrt{2}\sigma_\epsilon}\right) - \operatorname{erf}\left(\frac{-\pi/3}{\sqrt{2}\sigma_\epsilon}\right)}, \quad y \in \left[-\frac{\pi}{3}, \frac{\pi}{3}\right] \tag{2}$$

where σ_ϵ is the standard deviation of the beam alignment error and $\operatorname{erf}(\cdot)$ is the error function [22]. Similar to our previous works [15], [23], we consider that the variance, $\sigma^2_{\epsilon_k}$, of the beam alignment error for channel state k is obtained from the Cramér Rao lower bound (CRLB) of angle-of-arrival (AoA) estimates and is expressed in terms of a function of two parameters as

$$\sigma^2_{\epsilon_k}(\phi, \gamma_k) = \frac{6}{\left(\frac{2\pi f_c d\cos(\phi)}{c}\right)^2 M\left(M^2-1\right)\gamma_k}, \tag{3}$$

where ϕ is the true AoA measured from the boresight and γ_k represents the uplink received SNR of the pilot signals with channel state k at a single BS antenna element. The parameters f_c , c, and d are the carrier frequency, the speed of light and the antenna element spacing, respectively. We assume half-wavelength spacing between the antenna elements. The term $G_e(\phi)$ represents the antenna element pattern along the azimuth and is characterized according to the 3GPP specifications [24] as

$$G_{\mathrm{e}}^{(dB)}(\phi) = G_{\max} - \min\left[12\left(\frac{\phi}{\varphi_e}\right)^2, A_m\right], \tag{4}$$

where $\phi \in \left[-\frac{\pi}{3}, \frac{\pi}{3}\right]$, $G_{\max} = 8$ dBi, $A_m = 30$ dB and $\varphi_e = 65^\circ$ are the maximum gain, the front-to-back ratio and the half-power beamwidth (HPBW), respectively, of the single element.

The term γ_k depends on the transmit power of the UE, besides other parameters, and is expressed as [15]

$$\gamma_k(\phi, r) = \frac{\widetilde{P}_u G_e(\phi)\, \varrho_k^{ul} L_k(r)}{\sigma_n^2}, \tag{5}$$

where $\widetilde{P}_u$ is the uplink transmit power, ϱ_k^{ul} is the fading gain experienced by the uplink pilot signals and σ_n^2 represents the noise power.

Since UEs are battery-operated devices and battery power is a critical resource, we consider that each UE employs power control for the transmission of uplink pilot signals [8]. Similar to the power control mechanism of 3GPP LTE, this paper adopts the fractional power control (FPC) scheme, where a UE sets its uplink transmit power based on the path-loss to its serving BS with an aim to invert the effects of the corresponding path-loss to a certain degree [25], [26]. The UE transmit power with FPC is expressed as [11]

$$\widetilde{P}_u = \begin{cases} P_0 r^{\alpha_k \eta} & \text{if} \quad P_0 r^{\alpha_k \eta} \leq P_u^{\max} \\ P_u^{\max} & \text{otherwise,} \end{cases} \tag{6}$$

where P_0 is the baseline transmit power before applying the power control and $\eta \in [0, 1]$ is the power control factor, which represents the degree of path-loss inversion. The value of P_0 depends on the amount of spectral resources available to a UE. We assume that the entire system bandwidth, W, is available for the transmission of pilot signals. Therefore, P_0 is calculated as $P_0 = PSD + 10\log_{10}(W)$, where PSD is the power spectral density whose value is chosen to be -100 dBm/Hz [11]. The term $P_u^{\max}$ is the maximum transmit power for a UE and its value is set to 23 dBm [12], [25], [26]. When $\eta = 0$, it is considered that power control is not applied and all the UEs transmit with a constant power $P_u^{\max}$. However, when $\eta = 1$, each UE attempts to fully invert the effects of the corresponding path-loss. FPC is realized in its true sense when $0 < \eta < 1$, which is considered in this paper.

To characterize the array pattern of a ULA in terms of the beam alignment error, ϵ, the 3GPP pattern approximation of [15], [23] is adopted since it effectively captures the effects of beam misalignment while remaining tractable. The approximated array pattern, $\widetilde{G}_A(\phi, \epsilon)$, is expressed as

$$\widetilde{G}_A(\phi, \epsilon) = \begin{cases} G_1(\phi)\, 10^{\frac{-3}{10}\left(\frac{2\epsilon}{\varphi_A}\right)^2} & \text{if } |\epsilon| \leq \Theta_A \\ G_2 & \text{if } \Theta_A \leq |\epsilon| \leq \pi, \end{cases} \tag{7}$$

where $G_1(\phi)$ is the peak main lobe gain corresponding to a specific ϕ and G_2 is the average side lobe gain. The terms Θ_A and φ_A represent the main lobe beamwidth of the 3GPP pattern approximation corresponding to a specific value of ϕ and the broadside HPBW of a ULA, respectively. The values of these parameters are computed as follows

$$\begin{aligned} G_1(\phi) &= G_e(\phi) M, \\ G_2 &= \frac{1}{M \sin^2\left(\frac{3\pi}{2M}\right)}, \\ \Theta_A &= (\varphi_A/2)\sqrt{(10/3)\log_{10}\left[G_1(\phi)/G_2\right]}, \\ \varphi_A &= \pi - 2\cos^{-1}\left(\frac{1.391}{\pi M d}\right), \end{aligned} \tag{8}$$

TABLE I
NOTATION AND DEFAULT SYSTEM PARAMETERS

Notation	Description	Value
λ_{B}	BS density	$50/\mathrm{km}^2$
λ_{u}	User density	$200/\mathrm{km}^2$
P_{d}	Downlink transmit power	30 dBm
$P_u^{\max}$	Max UE transmit power	23 dBm
f_{c}	Carrier frequency	28 GHz
W	Bandwidth	1 GHz
$\alpha_{\mathrm{L}}, \alpha_{\mathrm{N}}$	LOS and NLOS path loss exponents respectively	2, 2.92
$C_{\mathrm{L}}, C_{\mathrm{N}}$	LOS and NLOS path loss intercepts respectively	-61.4 dB, -72 dB
$N_{\mathrm{L}}, N_{\mathrm{N}}$	Nakagami shape parameters for LOS and NLOS signals	3, 2
σ_n^2	Noise power	-174 dBm/Hz + $10\log_{10}(W)$ + 10 dB
$\mathcal{P}_{LOS}$, R_B	LOS ball model parameters	0.2, 200 m

The values of different system parameters along with their notation are tabulated in Table I. As mentioned in [15], the BS density considered in this paper corresponds to a noise-limited network. Hence, we only consider the SNR in this paper and do not deal with the out-of-cell interference.

III. Downlink SNR Coverage Probability and Uplink Power Control

This section describes how the downlink SNR coverage probability with imperfect alignment is obtained analytically when the pilot signals, used for downlink channel estimation, are transmitted by the UE using uplink power control.

The downlink SNR coverage probability, $\mathcal{C}(\tau)$, represents the probability that the downlink SNR for any UE in the network is greater than a certain threshold τ. Conditioned on channel state k, the conditional downlink SNR coverage, $\mathcal{C}_k(\tau)$, for the typical UE is expressed as

$$\mathcal{C}_k(\tau) = \mathbb{P}\left(\frac{P_{\mathrm{d}}\, \widetilde{G}_A(\phi, \epsilon)\, \varrho_k^{dl} L_k(r)}{\sigma_n^2} > \tau \;\middle|\; k\right), \tag{9}$$

where ϱ_k^{dl} denotes the downlink channel gain due to small-scale fading with channel state k. In our previous work [15], we showed that $\mathcal{C}_k(\tau)$ in (9) can be evaluated using the conditional distribution of ϵ, i.e., $f_{\epsilon|\phi,r}(y|\,\phi, r)$, as

$$\begin{aligned} \mathcal{C}_k(\tau) := &- \sum_{n=1}^{N_k} (-1)^n \binom{N_k}{n} \\ &\times \int_{r=0}^{\infty} \int_{\phi=-\frac{\pi}{3}}^{\frac{\pi}{3}} \int_{\epsilon=-\frac{\pi}{3}}^{\frac{\pi}{3}} e^{\left(\frac{-\beta_k n \tau \sigma_n^2}{P_{\mathrm{d}} \widetilde{G}_A(\phi,\epsilon) L_k(r)}\right)} \\ &\times f_{\epsilon|\phi,r}(y|\,\phi, r) f_\phi(\phi)\, \hat{f}_k(r)\, \mathrm{d}\epsilon\, \mathrm{d}\phi\, \mathrm{d}r, \end{aligned} \tag{10}$$

where $\beta_k = N_k (N_k!)^{\frac{-1}{N_k}}$ and $\hat{f}_k(r)$ is given in the Appendix. Moreover, the authors in [15] also showed that $f_{\epsilon|\phi,r}(y|\,\phi, r)$, obtained from (2) – (5), under Nakagami fading becomes a

truncated and scaled Student's t-distribution with PDF expressed as

$$f_{\epsilon|\phi,r}\left(y|\,\phi,r\right) := \frac{\frac{1}{\delta(\phi,r)} f_t\left(\frac{y}{\delta(\phi,r)}\right)}{F_t\left(\frac{\pi/3}{\delta(\phi,r)}\right) - F_t\left(-\frac{\pi/3}{\delta(\phi,r)}\right)}, \tag{11}$$

where $y \in [-\pi/3, \pi/3]$ and $\delta\left(\phi, r\right)$ is the scaling factor. The terms $f_t\left(\cdot\right)$ and $F_t\left(\cdot\right)$ represent the PDF and the cumulative distribution function (CDF), respectively, of the standardized t-distribution.

The value of the scale factor $\delta\left(\phi, r\right)$ also depends on the UE transmit power besides ϕ and r. In [15], a constant UE transmit power (i.e., $P_u^{\max}$) was considered, which rendered the expression of $\delta\left(\phi, r\right)$ as

$$\delta\left(\phi, r\right) = \sqrt{\frac{6\sigma_n^2}{\left(\frac{2\pi f_c d\cos(\phi)}{c}\right)^2 M\left(M^2-1\right) P_u^{\max} G_e\left(\phi\right) L_k\left(r\right)}}. \tag{12}$$

However, when uplink power control of the form of (6) is utilized, $\delta\left(\phi, r\right)$ becomes dependent on the power control factor, η, and its expression becomes different than (12) as explained in the following. The inequality $P_0 r^{\alpha_k \eta} \leq P_u^{\max}$ that defines the subdomain interval in (6) can be rewritten as $r \leq \left(\frac{P_u^{\max}}{P_0}\right)^{\frac{1}{\alpha_k \eta}}$. Using the indicator functions, the piece-wise function of (6) can be equivalently expressed as

$$\begin{aligned}\widetilde{P}_u = P_0\ r^{\alpha_k \eta} \mathbb{1}\left(r \leq \left(\frac{P_u^{\max}}{P_0}\right)^{\frac{1}{\alpha_k \eta}}\right) \\ + P_u^{\max}\ \mathbb{1}\left(r > \left(\frac{P_u^{\max}}{P_0}\right)^{\frac{1}{\alpha_k \eta}}\right),\end{aligned} \tag{13}$$

where $\mathbb{1}$ is the indicator function. Replacing the constant UE transmit power of $P_u^{\max}$ in (12) with the FPC-based UE transmit power of $\widetilde{P}_u$ given in (13), $\delta\left(\phi, r\right)$ can be expressed as (14), shown at the top of the next page.

The total downlink SNR coverage, $\mathcal{C}\left(\tau\right)$, with imperfect beam alignment and considering uplink power control is obtained from the law of total probability as $\mathcal{C}\left(\tau\right) = \sum_k \mathcal{A}_k \mathcal{C}_k\left(\tau\right)$ where $\mathcal{C}_k\left(\tau\right)$ is evaluated analytically using (10), (11) and (14) while $\mathcal{A}_k$, the probability of association with a BS of the k^{th} channel state, is given in the Appendix.

IV. Results and Discussion

This section illustrates how utilization of the FPC for the transmission of uplink pilot signals affects the the downlink SNR coverage of a mm-wave cellular network in the presence of beam alignment errors. Also, the analytical results of Section III are substantiated using Monte-Carlo simulations, which consist of 50,000 trials. For the simulations, the beam alignment errors are generated using (2) – (6) and the downlink SNR coverage for k^{th} channel state is obtained using (9) by considering that $\varrho_k^{dl} = \varrho_k^{ul}$ for each trial because of channel reciprocity.

Fig. 1 compares the downlink SNR coverage probability with imperfect beam alignment for two different values of the uplink power control factor, η (i.e., $\eta = 0.6$ and $\eta = 0.7$). Our choice for these values of η is motivated by [14]. Analytical curves in Fig. 1 obtained using both values of η match well with the corresponding simulated curves, thus, establishing the accuracy of the analytical model developed in Section III. For context, the simulated and analytical curves are also shown for two reference cases: the downlink SNR coverage with imperfect alignment obtained using $P_u^{\max}$ for the transmission of uplink pilots and the downlink SNR coverage with perfect alignment.[1] By comparison of the perfect and the imperfect alignment (with $P_u^{\max}$) curves, the authors in [15] showed that the beam alignment errors degrade the SNR coverage considerably in the low SNR regime whereas the effect of such errors is negligible for high SNR regime. Below, we investigate how the FPC affects these results.

With imperfect beam alignment, it is observed that the downlink SNR coverage obtained using $P_u^{\max}$ without FPC for the uplink pilots serves as an upper bound for the other imperfect alignment curves. This is trivial since the highest transmit power for the transmission of uplink pilots results in the lowest value of the corresponding downlink beam alignment error, as per (2) – (6). Moreover, when the FPC is utilized, a higher value of η generally results in a better downlink SNR coverage as compared to smaller values of η.

Nevertheless, when the SNR threshold, τ, is quite small (i.e., $\tau < -15$ dB in this case), both $\eta = 0.6$ and $\eta = 0.7$ result in the same downlink SNR coverage as with the constant uplink transmit power $P_u^{\max}$ without FPC. The reason is that such small values of τ are representative of NLOS UEs that are at a considerable distance from their respective serving BSs. For these UEs, the path-loss is significant because of the large link distance and the NLOS channel. Consequently, utilizing FPC even with a small value of η (e.g., $\eta = 0.6$) results in such UEs transmitting the pilot signals at the maximum possible power level, i.e., $P_u^{\max}$, according to (6).

However, for other values of τ (e.g., $\tau > -15$ dB for $\eta = 0.6$), the difference between imperfect alignment curves based on FPC and $P_u^{\max}$ becomes quite noticeable. This is because transitioning towards a high SNR regime, i.e., -15 dB $< \tau <$ 10 dB, corresponds to reducing the link distance between a UE and its serving BS. As a result, the path-loss also reduces comparatively and with FPC, the UEs are able to transmit their pilot signals at a lower power level than $P_u^{\max}$. A reduction in the transmit power, $\widetilde{P}_u$, of the uplink pilot signals reduces the received SNR correspondingly at the BS for downlink channel estimation. This sequentially causes the downlink beam alignment errors to increase, as per (2) – (3). Accordingly, the downlink SNR coverage with imperfect alignment degrades for the aforementioned values of τ when FPC is used for the transmission of uplink pilot signals.

For both the FPC-based curves, it is further observed that their respective difference from the $P_u^{\max}$-based curve is maximum at around $\tau = 10$ dB for the BS density and

[1]The analytical curves for these two reference cases are obtained using the t-distribution based approach mentioned in our earlier work [15].

$$\delta\left(\phi, r\right) = \sqrt{\frac{6\sigma_n^2}{\left(\frac{2\pi f_c d \cos(\phi)}{c}\right)^2 M\left(M^2-1\right)\left[P_0\ r^{\alpha_k \eta}\mathbb{1}\left(r \leq \left(\frac{P_u^{\max}}{P_0}\right)^{\frac{1}{\alpha_k \eta}}\right) + P_u^{\max}\ \mathbb{1}\left(r > \left(\frac{P_u^{\max}}{P_0}\right)^{\frac{1}{\alpha_k \eta}}\right)\right] G_e\left(\phi\right) L_k\left(r\right)}}. \tag{14}$$

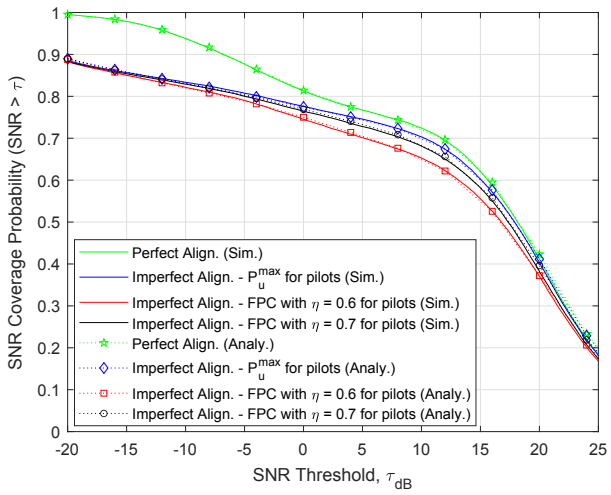

Fig. 1. Downlink SNR coverage probability with two different values of the uplink power control factor, η. Number of BS antennas $(M) = 32$, BS density $(\lambda_B) = 50/\text{km}^2$.

the number of antennas under consideration. This value of τ depicts the average achievable SNR at the boundary of the LOS ball and represents both the NLOS and the LOS UEs, which are near the boundary of the LOS ball but strictly inside it [15]. Here, the increased gap between the $P_u^{\max}$-based and the FPC-based curves is because of the LOS UEs. The LOS UEs experience much less path-loss as compared to the NLOS UEs for the same link distance. Therefore, with FPC, the LOS UEs use much lower power levels (as compared to $P_u^{\max}$) for the transmission of uplink pilot signals. The reduced SNR of the uplink pilot signals consequently increases the downlink beam alignment errors, which degrade the downlink SNR coverage.

For τ >10 dB, the aforementioned gap between the $P_u^{\max}$-based curve and the FPC-based curves starts to narrow down. This is because the high SNR regime represents UEs that are deep inside the LOS ball, where the path-loss is much less due to the short link distances and the effect of beam alignment errors is not significant for large values of τ, as discussed above. Though the UEs with such short link distances transmit their pilot signals with reduced power levels, the reduction in the power level is not enough to cause significant beam alignment errors.

In summary, the above observations for imperfect beam alignment illustrate that the use of FPC for the transmission of uplink pilots does not affect the downlink SNR coverage of distant NLOS UEs. However, the same does not hold for the LOS UEs. Moreover, as the link distance for the LOS UEs reduces, the effect of FPC also diminishes. Additionally, the downlink SNR coverage considering FPC with η =0.7 is almost the same as the one with the constant uplink transmit power of $P_u^{\max}$. Such an observation shows that the use of FPC can result in conserving power at the UE side without significant loss in the downlink SNR coverage. Below, we analyze this aspect.

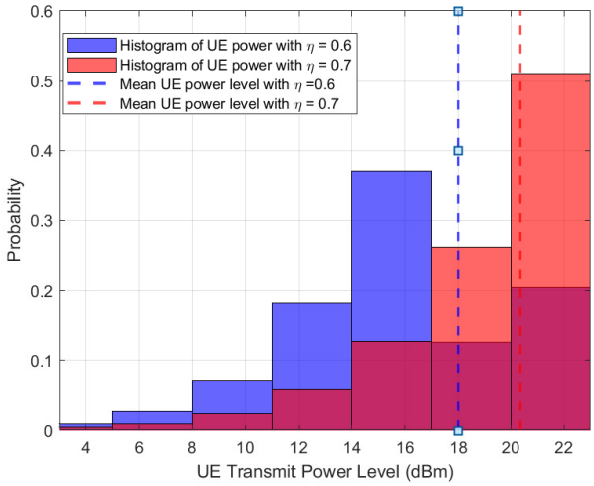

Fig. 2. Histogram plot of the UE transmit power levels with FPC for two different values of the power control factor (η). Maximum UE transmit power level $(P_u^{\max})$ =23 dBm, BS density $(\lambda_B) = 50/\text{km}^2$. Results obtained from simulations.

Fig. 2 shows the histogram plots of the UE transmit powers with FPC for $\eta = 0.6$ (blue) and $\eta = 0.7$ (orange), where the bin width along the horizontal axis is set to 3 dBm. The bin heights along the vertical axis represent the percentage of UEs transmitting within the particular power levels, which are specified by the respective bins edges. The purple color indicates the overlap of the two histograms. Also shown are the mean UE transmit power levels for the two values of η. When $\eta = 0.6$, it is observed that the mean UE transmit power level is almost 18 dBm and only 20% of the UEs transmit at power levels greater than or equal to 20 dBm. This means that 80% of the UEs transmit at power levels that are at least 3 dB less than the maximum power level of $P_u^{\max}$ = 23 dBm. This amounts to significant power savings at the UE side.

Moreover, when $\eta = 0.7$, the mean UE transmit power level is found to be about 20.36 dBm, which is almost 3 dB less than $P_u^{\max}$. Additionally, only about 51% of the UEs transmit at power levels greater than or equal to 20 dBm. This implies that with $\eta = 0.7$, still almost half of the UEs transmit at power levels, which are less than half of $P_u^{\max}$. These observations corroborate our earlier claim that when FPC is utilized for the transmission of uplink pilot signals, substantial power savings

can be achieved at the UE side without degrading the downlink performance when the beam alignment errors are accounted for.

V. Conclusion

This paper studies the effects of the uplink FPC on the downlink SNR coverage of a mm-wave cellular network in the presence of beam alignment errors. The FPC is utilized by the UEs to transmit pilot signals, which are used by the BS to estimate the downlink beamforming direction for data transmission. The downlink beam alignment errors depend on the SNR of the uplink pilot signals. Our results indicate that the use of FPC for uplink pilot transmission does not affect the downlink SNR of distant NLOS UEs. However, for the LOS UEs, the downlink achievable SNR degrades when the FPC is utilized. Moreover, this deterioration for LOS UEs diminishes as the link distance gets shorter. Nevertheless, with FPC, the use of a high power control factor does not cause a significant loss in the downlink SNR coverage with imperfect alignment. However, the power savings at the UE side are significant when FPC is utilized.

Appendix

$\hat{f}_k(r)$, the conditional PDF of the distance between the typical UE and its serving BS, conditioned on the event that the serving BS belongs to the k^{th} channel state, is expressed as [19]

$$\hat{f}_k(r) = \frac{f_k(r)}{\mathcal{A}_k} \exp\left(-2\pi\lambda_{\text{B}} \int_0^{\chi_k(r)} t\left(1-\mathcal{P}_k(t)\right) \mathrm{d}t\right), \tag{15}$$

where $\chi_{\text{L}}(r) = \left(\frac{C_{\text{N}}}{C_{\text{L}}}\right)^{\frac{1}{\alpha_{\text{N}}}} (r)^{\frac{\alpha_{\text{L}}}{\alpha_{\text{N}}}}$ and $\chi_{\text{N}}(r) = \left(\frac{C_{\text{L}}}{C_{\text{N}}}\right)^{\frac{1}{\alpha_{\text{L}}}} (r)^{\frac{\alpha_{\text{N}}}{\alpha_{\text{L}}}}$. The factor $f_k(r)$, the PDF of the distance from the typical UE to the closest BS of the k^{th} channel state, and $\mathcal{A}_k$ are evaluated respectively as [19]

$$f_k(r) = 2\pi\lambda_{\text{B}}\, r\mathcal{P}_k(r) \exp\left(-2\pi\lambda_{\text{B}} \int_0^{r} r\mathcal{P}_k(r)\, \mathrm{d}r\right), \tag{16}$$

$$\mathcal{A}_k = \int_0^{\infty} f_k(r) \exp\left(-2\pi\lambda_{\text{B}} \int_0^{\chi_k(r)} t\left(1-\mathcal{P}_k(t)\right) \mathrm{d}t\right) \mathrm{d}r. \tag{17}$$

References

[1] T. S. Rappaport, G. R. MacCartney, M. K. Samimi, and S. Sun, "Wide-band millimeter-wave propagation measurements and channel models for future wireless communication system design," *IEEE Trans. Commun.*, vol. 63, no. 9, pp. 3029–3056, Sep. 2015.

[2] S. Singh, M. N. Kulkarni, A. Ghosh, and J. G. Andrews, "Tractable model for rate in self-backhauled millimeter wave cellular networks," *IEEE J. Sel. Areas Commun.*, vol. 33, no. 10, pp. 2196–2211, Oct. 2015.

[3] A. Ghosh *et al.*, "Millimeter-wave enhanced local area systems: A high-data-rate approach for future wireless networks," *IEEE J. Sel. Areas Commun.*, vol. 32, no. 6, pp. 1152–1163, Jun. 2014.

[4] M. R. Akdeniz *et al.*, "Millimeter wave channel modeling and cellular capacity evaluation," *IEEE J. Sel. Areas Commun.*, vol. 32, no. 6, pp. 1164–1179, Jun. 2014.

[5] J. G. Andrews, T. Bai, M. N. Kulkarni, A. Alkhateeb, A. K. Gupta, and R. W. Heath, "Modeling and analyzing millimeter wave cellular systems," *IEEE Trans. Commun.*, vol. 65, no. 1, pp. 403–430, Jan. 2017.

[6] I. Ahmed *et al.*, "A survey on hybrid beamforming techniques in 5G: Architecture and system model perspectives," *IEEE Commun. Surveys Tuts.*, vol. 20, no. 4, pp. 3060–3097, 4th Quart., 2018.

[7] H. Wang, J. Fang, P. Wang, G. Yue, and H. Li, "Efficient beamforming training and channel estimation for millimeter wave OFDM systems," *IEEE Trans. Wireless Commun.*, vol. 20, no. 5, pp. 2805–2819, May 2021.

[8] P. Baracca, L. G. Giordano, A. Garcia-Rodriguez, G. Geraci, and D. López-Pérez, "Downlink performance of uplink fractional power control in 5G massive MIMO systems," in *Proc. IEEE Global Commun. Conf. Workshops*, 2018, pp. 1–6.

[9] S. Kusaladharma, W. Zhu, and W. Ajib, "Stochastic geometry-based modeling and analysis of massive MIMO-enabled millimeter wave cellular networks," *IEEE Trans. Commun.*, vol. 67, no. 1, pp. 288–301, Jan. 2019.

[10] S. Singh, X. Zhang, and J. G. Andrews, "Joint rate and SINR coverage analysis for decoupled uplink-downlink biased cell associations in hetnets," *IEEE Trans. Wireless Commun.*, vol. 14, no. 10, pp. 5360–5373, Oct. 2015.

[11] M. Di Renzo and P. Guan, "Stochastic geometry modeling and system-level analysis of uplink heterogeneous cellular networks with multi-antenna base stations," *IEEE Trans. Commun.*, vol. 64, no. 6, pp. 2453–2476, Jun. 2016.

[12] L. Zhang, W. Nie, G. Feng, F.-C. Zheng, and S. Qin, "Uplink performance improvement by decoupling uplink/downlink access in hetnets," *IEEE Trans. Veh. Technol.*, vol. 66, no. 8, pp. 6862–6876, 2017.

[13] N. A. Muhammad, N. I. A. Apandi, Y. Li, and N. Seman, "Uplink performance analysis for millimeter wave cellular networks with clustered users," *IEEE Trans. Veh. Technol.*, vol. 69, no. 6, pp. 6178–6188, Jun. 2020.

[14] O. Onireti, A. Imran, and M. A. Imran, "Coverage, capacity, and energy efficiency analysis in the uplink of mmWave cellular networks," *IEEE Trans. Veh. Technol.*, vol. 67, no. 5, pp. 3982–3997, May 2018.

[15] M. S. Zia, D. M. Blough, and M. A. Weitnauer, "Effects of SNR-dependent beam alignment errors on millimeter-wave cellular networks," *IEEE Trans. Veh. Technol.*, vol. 71, no. 5, pp. 5216–5230, May 2022.

[16] M. Haenggi, *Stochastic Geometry for Wireless Networks*. Cambridge, U.K.: Cambridge Univ. Press, 2012.

[17] R. W. Heath, N. González-Prelcic, S. Rangan, W. Roh, and A. M. Sayeed, "An overview of signal processing techniques for millimeter wave MIMO systems," *IEEE J. Sel. Topics Signal Process.*, vol. 10, no. 3, pp. 436–453, Apr. 2016.

[18] M. Rebato, J. Park, P. Popovski, E. De Carvalho, and M. Zorzi, "Stochastic geometric coverage analysis in mmWave cellular networks with realistic channel and antenna radiation models," *IEEE Trans. Commun.*, vol. 67, no. 5, pp. 3736–3752, May 2019.

[19] M. Shi, K. Yang, C. Xing, and R. Fan, "Decoupled heterogeneous networks with millimeter wave small cells," *IEEE Trans. Wireless Commun.*, vol. 17, no. 9, pp. 5871–5884, Sep. 2018.

[20] A. Thornburg and R. W. Heath, "Ergodic capacity in mmWave ad hoc network with imperfect beam alignment," in *Proc. IEEE Military Commun. Conf. (MILCOM)*, Oct. 2015, pp. 1479–1484.

[21] M. Cheng, J. Wang, Y. Wu, X. Xia, K. Wong, and M. Lin, "Coverage analysis for millimeter wave cellular networks with imperfect beam alignment," *IEEE Trans. Veh. Technol.*, vol. 67, no. 9, pp. 8302–8314, Sep. 2018.

[22] M. Abramowitz and I. A. Stegun, Eds., *Handbook of Mathematical Functions, with Formulas, Graphs, and Mathematical Tables,*. Washington, DC, USA: NBS, 1964.

[23] M. S. Zia, D. M. Blough, and M. A. Weitnauer, "Coverage in millimeter-wave networks with SNR-dependent beam alignment errors," in *Proc. IEEE Veh. Technol. Conf. (VTC-Spring)*, May 2020, pp. 1–5.

[24] *Technical Specification Group Radio Access Network; Study of radio frequency (RF) and electromagnetic compatibility (EMC) requirements for active antenna array system (AAS) base station (Release 12)*, document 3GPP TR 37.840, 3GPP, Dec. 2013.

[25] J. Góra, K. I. Pedersen, A. Szufarska, and S. Strzyz, "Cell-specific uplink power control for heterogeneous networks in LTE," in *Proc. IEEE Veh. Technol. Conf.*, 2010, pp. 1–5.

[26] R. Müllner, C. F. Ball, K. Ivanov, J. Lienhart, and P. Hric, "Performance comparison between open-loop and closed-loop uplink power control in UTRAN LTE networks," in *Proc. ACM Int. Conf. Wireless Commun. Mobile Comput.*, 2009, pp. 1410–1416.